Weierstraß-Institut
für Angewandte Analysis und Stochastik

Leibniz-Institut im Forschungsverbund Berlin e. V.

Preprint ISSN 2198-5855

Multiscale modeling of vascularized tissues via non-matching immersed methods

Luca Heltai[1], Alfonso Caiazzo[2]

submitted: November 21, 2018

[1] International School for Advanced Studies (SISSA)
Via Bonomea 265
34236, Trieste, Italy
E-Mail: luca.heltai@sissa.it

[2] Weierstrass Institute
Mohrenstr. 39
10117 Berlin, Germany
E-Mail: alfonso.caiazzo@wias-berlin.de

No. 2555
Berlin 2018

2010 *Mathematics Subject Classification.* 74F10, 74Q99, 74S05, 74G15.

Key words and phrases. Immersed boundary method, finite element, vascularized tissue, fluid-structure interaction, multi-scale methods.

Edited by
Weierstraß-Institut für Angewandte Analysis und Stochastik (WIAS)
Leibniz-Institut im Forschungsverbund Berlin e. V.
Mohrenstraße 39
10117 Berlin
Germany

Fax: +49 30 20372-303
E-Mail: preprint@wias-berlin.de
World Wide Web: http://www.wias-berlin.de/

Multiscale modeling of vascularized tissues via non-matching immersed methods

Luca Heltai, Alfonso Caiazzo

Abstract

We consider a multiscale approach based on immersed methods for the efficient computational modeling of tissues composed of an elastic matrix (in two or three-dimensions) and a thin vascular structure (treated as a co-dimension two manifold) at a given pressure. We derive different variational formulations of the coupled problem, in which the effect of the vasculature can be surrogated in the elasticity equations via singular or hyper-singular forcing terms. These terms only depends on information defined on co-dimension two manifolds (such as vessel center line, cross sectional area, and mean pressure over cross section), thus drastically reducing the complexity of the computational model. We perform several numerical tests, ranging from simple cases with known exact solutions to the modeling of materials with random distributions of vessels. In the latter case, we use our immersed method to perform an in silico characterization of the mechanical properties of the effective biphasic material tissue via statistical simulations.

1 Introduction

This paper is motivated by mathematical and computational modeling in the context of tissue imaging, such as Magnetic Resonance Elastography (MRE), a quantitative imaging technique sensitive to the mechanical properties of living tissues. In MRE, the tissue undergoes external harmonic excitations, such as shear or compression waves, and Magnetic Resonance Imaging is used to recover the mechanical response of the tissue in terms of the internal displacement. These data, combined with a mathematical model of the underlying tissue dynamics, are then employed to characterize the tissue – in vivo and non invasively – in order to identify and localize tissue anomalies, such as cancer or fibrosis (see, e.g., [24, 29, 20, 30]).

Recent experimental studies have been dedicated to the potential of MRE to characterize intrinsic properties of biphasic tissues (e.g., brain and liver), aiming at the non invasive diagnosis of pressure related diseases (see, e.g., [18, 19]). To this aim, efficient models able to describe both phases (solid matrix and fluid vasculature) are necessary. From the computational point of view, fully resolved biphasic models, i.e., accounting for the coupling between the tissue and fluid vasculature at the microscale, are practically unfeasible. On the one hand, the elevate geometrical complexity would lead to excessive computational cost and, on the other hand, image resolution used in MRE (of the order of millimeters) does not allow to reconstruct in full detail the vasculature. The goal of this work is to propose a novel mathematical multiscale model for the mechanics of a biphasic tissue, (composed of an elastic matrix and a thin fluid vasculature) in which the vasculature (microscale) is not explicitly discretized, but it is immersed in the elasticity problem describing the matrix dynamics at the macroscale.

To this aim, we use an approach based on the Immersed Boundary Method (IBM), in order to account for complex (one-dimensional) structures within two- and three-dimensional elastic materials.

DOI 10.20347/WIAS.PREPRINT.2555 Berlin 2018

The Immersed Boundary Method was introduced by Peskin in [25], to study the blood flow around heart valves (see also [26], or the review [22]), and evolved into a large variety of methods and algorithms. The main idea behind this technique is to address complex fluid-structure interaction problems by formulating them on a fixed background fluid problem, with the addition of singular source terms that take into account the presence of the solid equations, removing the requirement that the position of the interfaces between the fluid and solid domains should be aligned with the computational mesh.

In the original Immersed Boundary Method [25] the singular source terms are formally written in terms of the Dirac delta distribution, and their discretization follows two possible routes: i) the Dirac delta distribution is approximated through a smooth function, or ii) the variational definition of the Dirac distribution is used directly in the Finite Element formulation of the problem. For finite difference schemes, the first solution is the only viable option, even though the use of smooth kernels may excessively smear the singularities, leading to large errors in the approximation [21]. In the context of finite elements, instead, both solutions are possible. The methods derived from the Immersed Finite Element Method (IFEM) still use approximations of the Dirac delta distribution through the Reproducing Kernel Particle Method (RKPM) [31].

Variational formulations of the IBM were introduced in [5, 7, 8, 12], and later generalised in [15] and [28], where the need to approximate Dirac delta distributions is removed by exploiting directly the weak formulation. Such formulations allow the solution of PDEs with jumps in the gradients without enriching the finite element space, and without introducing approximations of the Dirac delta distribution. In the context of 3D-1D multiscale models, an approach using techniques similar to the IBM has been described in [11, 10] for the case of diffusion equations. In this case, a diffusion problem was solved on both the 3D and on the 1D domains, considering, additionally, the 1D vasculature as a source of nutrients for the 3D tissue. This approach has been recently extended to the case of a 3D porous media (Darcy) coupled to an immersed vasculature, resolving the flow in the vascular network via a (0D) lumped parameter model [9].

In this paper, we consider the case of a 3D (or 2D) elastic matrix with an immersed 1D (resp. 0D) vasculature with a given fluid pressure, i.e., under the assumption that the diameter of the fluid vessel is much smaller than the size of the characteristic domain.

In the variational formulation, the effect of the fluid is then included in the elasticity equations by means of a singular source term on a lower dimensional manifold. We begin by analyzing a singular formulation in which the source term is concentrated on the vessel boundary. Next, we discuss a *hyper-singular* alternative, in which the immersed source term is applied only at the vessel centerline (a co-dimension two manifold), thus reducing drastically the computational effort.

The multiscale model will be derived starting from a 2D-0D axis-symmetric case and subsequently extended to the general 3D-1D situation. We perform different numerical tests, validating the model in a simple setting in which an analytical solution is available, and investigating the statistical effective behavior of a biphasic material with random vessel distribution as a function of elastic and geometrical parameters. We focus on the effective tissue dynamics assuming a steady known fluid pressure in the vasculature.

An extension of this model including a two-way coupling with an active one-dimensional vasculature (e.g., using the approach described in [23]) is currently under investigation and will be subject of a future work.

The rest of the paper is organized as follows. In Section 2 we discuss the two-dimensional case, starting from a model problem with known exact solution. The approach is extended in Section 3 to the three dimensions, while its discretization is discussed in Section 4. Numerical results are presented

in Section 5, while Section 6 draws some conclusions.

2 The two-dimensional model

2.1 A simple problem setting

We consider the situation of a biphasic tissue composed of an elastic matrix and thin blood vessels, under the assumption that the vessel diameters are much smaller of the typical size of the surrounding matrix. To fix the ideas, we start with the derivation for a two-dimensional model problem, considering a single vessel. Assuming that the vessels are small compared to the elastic matrix, and that long term interaction can be neglected, the arguments can be extended also to the general domains and multiple vessels.

Let $a > 0$, and let us introduce the set

$$B^a = \{\mathbf{x} \mid \|\mathbf{x}\| \leq a\}$$

describing a circle of radius a (which will be also referred to as *vessel*). Next, let $\Omega \subset \mathbb{R}^2$ and let us introduce the *tissue* domain $\Omega^a = \Omega \backslash B^a$. We assume that the boundary of Ω is decomposed as

$$\partial\Omega = \Gamma_D \cup \Gamma_N \,,$$

and we define $\Gamma := \partial B^a$ to be the vessel boundary, and we denote with $\mathbf{n}$ the normal vector to Γ pointing outwards the tissue domain (see, e.g., the sketches in Figure 1).

This setting represents the case of a tissue that extends indefinitely along the z-direction with an embedded cylindrical vessel with cross-section equal to B^a. We assume that the presence of a flow

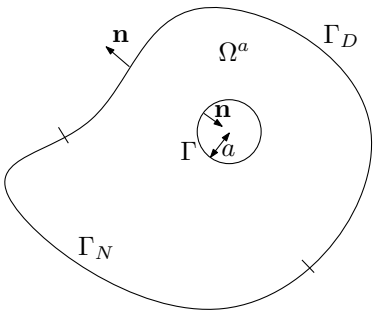

Figure 1: An example of a domain Ω with a single vessel of radius a.

inside the vessel can be modeled as a constant *excess pressure* $\bar{p}$, that represents the difference in pressure between the interior part of the vessel, and the surrounding elastic matrix. The excess pressure represents the force per unit area that the vessel exerts on the elastic matrix, and we assume that this force is directed along the normal to the vessel.

We now consider the following problem:

Problem 2.1 (2D on Ω^a) *Given the excess pressure $\overline{p} > 0$, find the displacement $\mathbf{u}^a : \Omega^a \to \mathbb{R}^2$*

solution to:

$$\begin{aligned} -\nabla \cdot \sigma(\mathbf{u}^a) &= 0, \quad \textit{in } \Omega^a \\ \mathbf{u}^a &= 0, \quad \textit{on } \Gamma_D \\ \sigma(\mathbf{u}^a)\mathbf{n} &= 0, \quad \textit{on } \Gamma_N \\ \sigma(\mathbf{u}^a)\mathbf{n} &= -\overline{p}\,\mathbf{n} \quad \textit{on } \Gamma \end{aligned} \tag{1}$$

The above system of equations describes the dynamics of a compressible, linear elastic material, where

$$\sigma(\mathbf{u}) := 2\mu e(\mathbf{u}) + \lambda I \operatorname{div} \mathbf{u}, \tag{2}$$

stands for the first Piola–Kirchoff stress tensor, $e(\mathbf{u}) = \frac{1}{2}\left(\nabla\mathbf{u} + \nabla\mathbf{u}^T\right)$ *denotes the symmetric part of the deformation gradient,* μ *and* λ *are the so called Lamé constants, and* I *is the identity matrix.*

Remark 2.1 *Notice that, using* (2)*, the normal component of the solid stress* $\sigma(\mathbf{u})\mathbf{n}$ *can be also written as* $\sigma(\mathbf{u})\mathbf{n} = (2\mu + \lambda)(\operatorname{div}\mathbf{u})\mathbf{n}$

Let us now introduce the functional spaces

$$V^a := \{\mathbf{v} \in (H^1(\Omega^a))^2, \text{ such that } \mathbf{v}|_{\Gamma_D} = \mathbf{0}\}, \tag{3}$$

Multiplying (1) with $\mathbf{v} \in V^a$ and integrating by parts yields a standard variational formulation of Problem 2.1:

Problem 2.2 (2D on Ω^a, variational) *Given the excess pressure* $\overline{p} > 0$*, find the displacement* $\mathbf{u}^a \in V^a$ *solution to:*

$$2\nu(e(\mathbf{u}^a), e(\mathbf{v}))_{\Omega^a} + \lambda(\operatorname{div}\mathbf{u}^a, \operatorname{div}\mathbf{v})_{\Omega^a} = \int_\Gamma \bar{p}\mathbf{n}\cdot\mathbf{v}\,\mathrm{d}\Gamma \quad \forall \mathbf{v} \in V^a, \tag{4}$$

where $(\cdot,\cdot)_{\Omega^a}$ *denotes the inner product in* $(L^2(\Omega^a))^2$*.*

2.2 Exact solution in the axis-symmetric case

In the special case where Ω is a circle of radius $R > a$ (see Figure 2), problem 1 can be solved analytically. Writing equation (1) in polar coordinates, simple symmetry arguments allow to conclude

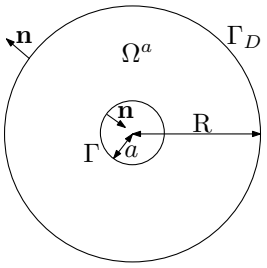

Figure 2: An example of an axi-symmetric domain Ω with a single vessel of radius a.

that the angular component of the solution vanishes, while the radial component depends only on the

distance from the vessel, i.e., $\mathbf{u}^a(\mathbf{x}) = u_\rho \frac{\mathbf{x}}{|\mathbf{x}|}$. The elasticity problem reduces therefore to an ODE for u_ρ, yielding the displacement

$$\mathbf{u}^a(\mathbf{x}) = \frac{\overline{p}a^2\left(R^2 - |\mathbf{x}|^2\right)}{2\left(R^2\mu + \lambda a^2 + \mu a^2\right)} \frac{\mathbf{x}}{|\mathbf{x}|^2}. \tag{5}$$

Figure 3(left) shows the behaviour of the radial displacement given by (5), varying the size a of the vessel.

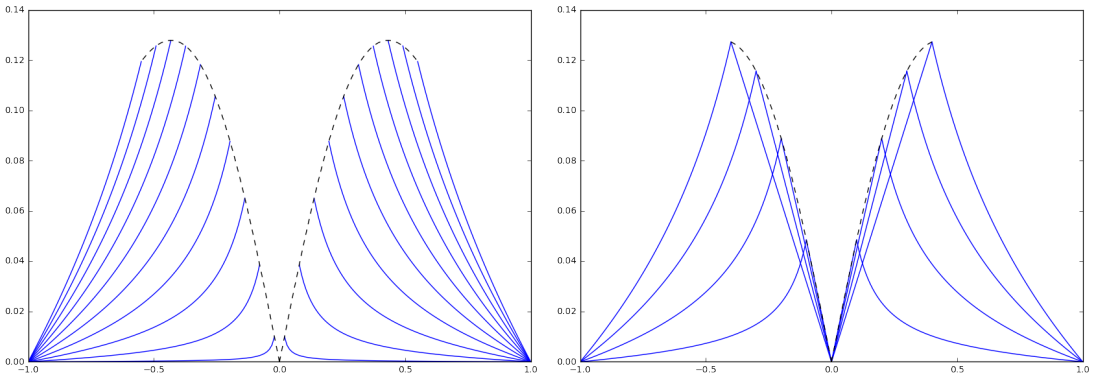

Figure 3: Left: Central sections of the radial component of the exact solution $\mathbf{u}_a$, for different values of the vessel radius $a \in [0.02, 0.55]$ (with $\lambda = \mu = 1$, $R = 1$, $p = 1$). Right: Central sections of the radial component of the exact solution $|u_\rho|$ to Problem 2.3, for different values of the vessel size $a = .1, .2, .3, .4$ ($\lambda = \mu = 1$, $R = 1$, $p = 1$).

We are interested in the situation where the radius of the vessel is small compared to the size of the tissue domain. Under the assumption $a \ll R$, we obtain the approximation:

$$\mathbf{u}^a|_\Gamma = \frac{\overline{p}a\left(R^2 - a^2\right)}{2R^2\mu + 2\lambda a^2 + 2\mu\varepsilon^2} \frac{\mathbf{x}}{|\mathbf{x}|} = -\frac{\overline{p}a}{2\mu}\mathbf{n} + O\left(\left(\frac{a}{R}\right)^2\right) \tag{6}$$

where we also used the fact that, on Γ, it holds $\dfrac{\mathbf{x}}{|\mathbf{x}|} = -\mathbf{n}$.

From (5)-(6), we conclude that the excess pressure $\overline{p}$ induces a radial deformation of the surrounding elastic matrix (normal to the vessel boundary) which is of the order of $\frac{\overline{p}a}{2\mu}$ on the vessel boundary and decays as $\frac{1}{|\mathbf{x}|}$.

2.3 A singular problem on the whole domain

Next, we aim at formulating an extension of the axi-symmetric problem on the whole domain Ω, and at introducing a forcing term so that the solution of the extended problems coincides with the solution $\mathbf{u}^a$, defined in (5), only outside of B^a.

In practice, we first extend the solution $\mathbf{u}^a$ inside B^a as a uniform deformation, i.e., linearly in the

distance from the origin (see Figure 3, right):

$$\mathbf{u}^{\Omega}(\mathbf{x}) = \begin{cases} \dfrac{\overline{p}\,(R^2 - |\mathbf{x}|^2)}{2\,(R^2\mu + \lambda a^2 + \mu a^2)}\,\dfrac{a^2\mathbf{x}}{|\mathbf{x}|^2} & |\mathbf{x}| \geq a \\ \\ \dfrac{\overline{p}\,(R^2 - a^2)}{2R^2\mu + 2\lambda a^2 + 2\mu a^2}\,\mathbf{x} & |\mathbf{x}| < a \end{cases} \tag{7}$$

The function $\mathbf{u}^{\Omega}$ defined in (7) is continuous across the vessel boundary Γ. However, the normal stress has a jump given by

$$g_a\mathbf{n} := [\![\sigma(\mathbf{u}^{\Omega})\mathbf{n}]\!]_{\Gamma} := \frac{R^2\overline{p}\,(\lambda + 2\mu)}{R^2\mu + \lambda a^2 + \mu a^2}\mathbf{n}\,. \tag{8}$$

Hence, in order to define an elasticity problem on Ω, whose solution is given by $\mathbf{u}^{\Omega}$, we will consider a fictitious elastic material defined on the whole domain, with same properties as the original one (defined in Ω^a), but subjected to a singular source term that imposes the jump $g_a\mathbf{n}$ in the normal stress. Namely, we consider the following problem:

Problem 2.3 (2D, singular) *Given an excess pressure $\overline{p} > 0$, find the distributional solution $\mathbf{u}$ to:*

$$\begin{aligned} -\nabla\cdot\sigma(\mathbf{u}) &= \mathbf{F}_a^S, && \textit{in } \Omega \\ \mathbf{u} &= 0, && \textit{on } \Gamma_D \\ \sigma(\mathbf{u})\mathbf{n} &= 0, && \textit{on } \Gamma_N \end{aligned} \tag{9}$$

with

$$\mathbf{F}_a^S(\mathbf{x}) := \int_{\Gamma} \delta(\mathbf{x} - \mathbf{y}) g_a\mathbf{n}(\mathbf{y})\,\mathrm{d}\Gamma_{\mathbf{y}}, \qquad \forall \mathbf{x} \in \Omega \tag{10}$$

where δ denotes the two-dimensional Dirac delta distribution and $\mathbf{y}$ stands for a local coordinate on the interface Γ.

In order to understand the definition of Problem 2.3, let us introduce the Sobolev space

$$V := \{\mathbf{v} \in (H^1(\Omega))^2, \text{ such that } \mathbf{v}|_{\Gamma_D} = \mathbf{0}\}\,,$$

denoting with $(\cdot,\cdot)$ the scalar product in $L^2(\Omega)$, and with $<\cdot,\cdot>$ the duality product between $H_0^1(\Omega)$ and its dual space $H^{-1}(\Omega)$. Multiplying (9) with a function $\mathbf{v} \in V$ and integrating by parts over Ω^a we obtain:

$$2\mu\,(e(\mathbf{u}), e(\mathbf{v}))_{\Omega^a} + \lambda\,(\operatorname{div}\mathbf{u}, \operatorname{div}\mathbf{v})_{\Omega^a} - (\sigma(\mathbf{u})\mathbf{n}, \mathbf{v})_{\Gamma} = 0\,. \tag{11}$$

Proceeding similarly, but considering a fictitious elasticity problem inside B^a with the same characteristics of the surrounding elastic matrix, we obtain

$$2\mu\,(e(\mathbf{u}), e(\mathbf{v}))_{B^a} + \lambda\,(\operatorname{div}\mathbf{u}, \operatorname{div}\mathbf{v})_{B^a} + (\sigma(\mathbf{u})\mathbf{n}, \mathbf{v})_{\Gamma} = 0 \tag{12}$$

where the signs of the last terms in (11) and (12) depend on the chosen orientation of the normal vector $\mathbf{n}$ (from the tissue towards the vessel). Summing (11) and (12), imposing continuity on the displacement and the given jump of the normal stress (8), we obtain the weak formulation:

Problem 2.4 (2D, singular, variational) *Given an excess pressure $\bar{p}$, find the solution $\mathbf{u} \in V$ such that*

$$(2\mu e(\mathbf{u}), e(\mathbf{v}))_{\Omega} + (\lambda \operatorname{div}\mathbf{u}, \operatorname{div}\mathbf{v})_{\Omega} = \int_{\Gamma} g_a\mathbf{n}\cdot\mathbf{v} \qquad \forall \mathbf{v} \in V. \tag{13}$$

Now, let us introduce the distributional definition of the two dimensional Dirac delta distribution, i.e.,

$$\int_\Omega \mathbf{v}(\mathbf{x})\delta(\mathbf{x}-\mathbf{y})\,\mathrm{d}x = \mathbf{v}(\mathbf{y}) \quad \forall \mathbf{v} \in V \cap C^0(\Omega), \forall \mathbf{y} \in \Omega\,. \tag{14}$$

Using (14), switching the order of integration, and interpreting the integral on Γ of functions in V in the sense of traces, it is possible to rewrite formally the term $\int_\Gamma g_a \mathbf{n}\cdot\mathbf{v}$ as

$$\begin{aligned}
&\int_\Gamma g_a(\mathbf{y})\mathbf{n}(\mathbf{y})\cdot \quad \mathbf{v}(\mathbf{y}) \qquad\qquad\qquad \mathrm{d}\Gamma_{\mathbf{y}} = \\
&\int_\Gamma g_a(\mathbf{y})\mathbf{n}(\mathbf{y})\cdot \int_\Omega \mathbf{v}(\mathbf{x})\delta(\mathbf{x}-\mathbf{y})\,\mathrm{d}x\,\mathrm{d}\Gamma_{\mathbf{y}} = \\
&\int_\Omega \int_\Gamma g_a\mathbf{n}(\mathbf{y})\delta(\mathbf{x}-\mathbf{y})\,\mathrm{d}\Gamma_{\mathbf{y}} \cdot \mathbf{v}(\mathbf{x})\,\mathrm{d}\mathbf{x} =: < \mathbf{F}_a^S, \mathbf{v} >,
\end{aligned} \tag{15}$$

where $\mathbf{F}_a^S$ is the singular forcing term introduced in (10).

For a detailed discussion on the behaviour of this distributional forcing term, see [17]. The term $\mathbf{F}_a^S$ is a distribution in $H^{-1}(\Omega)$, and was introduced originally in [6] and later generalized in [12, 8, 16] as a variational formulation of the Immersed Boundary Method [27], to approximate fluid structure interaction problems using non-matching grids between the immersed structure and the surrounding fluid.

2.4 The hypersingular problem

The variational formulation introduced in (13) allows to reformulate the coupled problem as an elasticity problem on the whole domain Ω without explicitly taking into account the boundary condition on the vessel boundary, so that, in the axi-symmetric case, the solution coincides with the exact one outside the vessel B^a. From the practical point of view, this approach might be used to employ a spatial discretization (mesh) that does not explicitly resolve in full detail the vessel boundary, hence considerably reducing the overall complexity, especially in the case of thin vessels. On the other hand, a discretization of the formulation described in Problem 2.3 still requires a characteristic mesh size that resolves the vessels boundary, in order to compute accurately enough the integral on Γ_a. For small to very small vessels sizes, this constrain might still yield an excessive computational cost.

To tackle this issue, we generalize our approach one step further. Namely, let us consider an additional parameter $\varepsilon > 0$, representing the *fictitious area of influence of the vessels*, and the corresponding circle B^ε of radius ε. We now look for a fictitious elasticity problem inside both B^a and B^ε, so that the solution coincides with the one defined in (5) only outside of the ball of radius $\max\{a,\varepsilon\}$ (see Figure 2.4). Moreover, we impose a jump of the normal stress on the (non-physical) boundary Γ_ε instead of on the vessel boundary Γ_a.

This fictitious problem can be constructed analogously to the one defined in Section 2.3. Namely, defining an extended – continuous – solution over the whole domain Ω, computing the jump of the normal stress across the boundary of B^ε and imposing this jump via a singular term in the elasticity equation. In this case, the jump to be imposed reads

$$g_\varepsilon := \frac{a^2}{\varepsilon^2}\frac{R^2\overline{p}\,(\lambda+2\mu)}{(R^2\mu+\lambda a^2+\mu a^2)} = \frac{a^2}{\varepsilon^2}g_a. \tag{16}$$

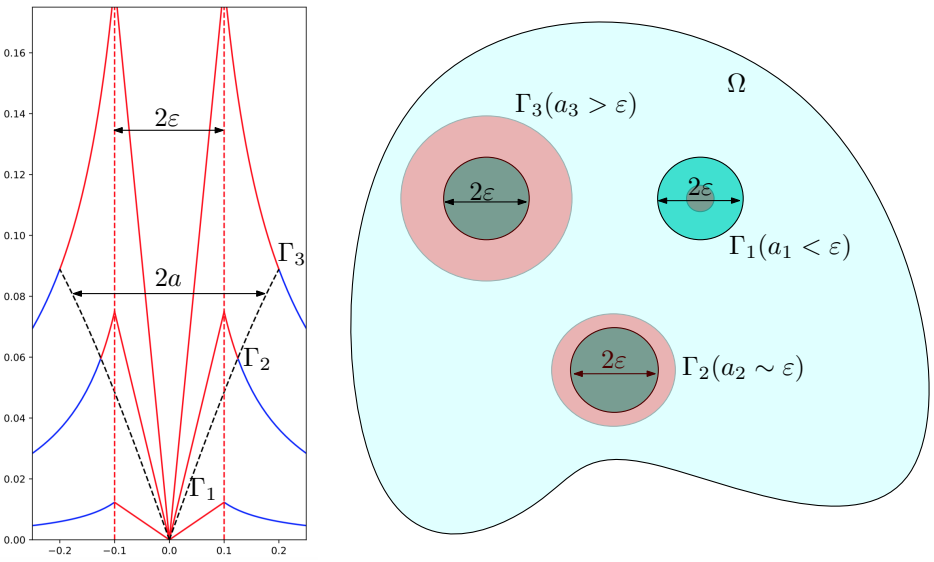

Figure 4: Example of vessel distribution with different radii a_i, and same fictitious area of influence ε.

It is worth noticing that (16) generalizes the formula previously derived in (8). In particular, the solution outside B^a reduces to (7) only if $\varepsilon \leq a$. When $\varepsilon > a$, the solution coincides with the exact one only outside of ε, and there is a region, corresponding to the area between ε and a, where the solution is unphysical.

The advantage of using (16), is that we can define arbitrarily the scale ε, that represents the *resolution* of interest, i.e., the relevant scale at which we want to approximate our singular forcing term. At a distance at least ε from the vessels, the solution coincides with the expected one, while inside the vessels, or inside a ball of radius ε from the vessel (whichever is bigger), the solution we obtain is unphysical.

The resolution at which we need to integrate over Γ_ε is now independent on the vessels size a, and, in particular, it can be fixed *a posteriori*, after a discretization strategy (and a mesh size) is defined for the domain Ω. This allows to define a forcing term in the limit for $\varepsilon \to 0$, independently on the vessel's size. In this case, the forcing term for a single vessel centered at the origin in the variational formulation would reduce to

$$\begin{aligned} \lim_{\varepsilon\to 0} \int_{\Gamma_\varepsilon} g_\varepsilon \mathbf{n}\cdot\mathbf{v}\,\mathrm{d}\Gamma &= \lim_{\varepsilon\to 0} \int_{B^\varepsilon} \frac{a^2}{\varepsilon^2} g_a \operatorname{div}\mathbf{v}\,\mathrm{d}\mathbf{x} \\ &= \pi a^2 g_a \operatorname{div}\mathbf{v}(\mathbf{0}), \quad \forall \mathbf{v}\in C^1(\Omega). \end{aligned} \tag{17}$$

Equation (17) defines the hyper-singular forcing term

$$\mathbf{F}^H(\mathbf{x}) := -\pi a^2 g_a \nabla\delta(\mathbf{x}), \tag{18}$$

so that

$$< \mathbf{F}^H, \mathbf{v} >:= \pi a^2 g_a \operatorname{div}\mathbf{v}(\mathbf{0}) \qquad \forall \mathbf{v}\in C^1(\Omega). \tag{19}$$

We remark here that $\mathbf{F}^H$ cannot be used *as-is* as a source term for our elasticity problem, since it does not belong to the space $H^{-1}(\Omega)$.

It is however possible to *mollify* the hyper singular formulation (18), by employing a smooth approximation of the Dirac delta distribution $\delta^{\varepsilon'}$, according to a small parameter ε', that again represents the

resolution at which we resolve our singular forcing terms. Although this new parameter is technically different from the one introduced in Equation (16), in the rest of the paper we will set $\varepsilon' = \varepsilon$, i.e., identifying the scale of interest with the radius of approximation of the Dirac delta distribution.

In particular, we consider approximations δ^ε of the Dirac delta distribution such that:

- $\delta^\varepsilon(\mathbf{x}-\mathbf{y}) = \delta^\varepsilon(\mathbf{y}-\mathbf{x})$
- $\int_{\Re^2} \delta^\varepsilon(\mathbf{x}-\mathbf{y})\,\mathrm{d}\mathbf{y} = \int_{B_\varepsilon(\mathbf{x})} \delta^\varepsilon(\mathbf{x}-\mathbf{y})\,\mathrm{d}\mathbf{y} = 1$
- $\delta^\varepsilon \in C^1(\Re^2)$
- $\int_{\Re^2} \nabla_{\mathbf{y}}\delta^\varepsilon(\mathbf{x}-\mathbf{y})\,\mathrm{d}\mathbf{y} = \int_{B_\varepsilon(\mathbf{x})} \nabla_{\mathbf{y}}\delta^\varepsilon(\mathbf{x}-\mathbf{y})\,\mathrm{d}\mathbf{y} = \mathbf{0}$.

and we defined the *mollified* forcing term

$$< \mathbf{F}^H_\varepsilon, \mathbf{v} >:= \int_\Omega \delta^\varepsilon(\mathbf{y})\pi a^2 g_a \,\mathrm{div}\,\mathbf{v}(\mathbf{y})\,\mathrm{d}\mathbf{y} \qquad \forall \mathbf{v} \in H^1(\Omega). \tag{20}$$

For a discussion on the properties of possible Dirac delta approximations to use, we refer the reader to the excellent review paper [21].

The above formula can be straightforwardly generalized to the case of N vessels, of radii a_i, $i = 1,\dots,N$ and centered in $\mathbf{x}_i$, $i = 1,\dots,N$. Introducing also the approximation $a \ll R$ for the definition of the stress jump, i.e.,

$$g_a\mathbf{n} = \frac{R^2\overline{p}\,(\lambda+2\mu)}{R^2\mu+\lambda a^2+\mu a^2}\mathbf{n} = \frac{2\mu+\lambda}{\mu}\overline{p} + O\left(\left(\frac{a}{R}\right)^2\right), \tag{21}$$

we obtain the hyper-singular forcing term

$$\mathbf{F}^H(\mathbf{x}) = -\sum_{i=1}^N \frac{2\mu+\lambda}{\mu}\pi a_i^2\overline{p}_i\,\nabla\delta(\mathbf{x}-\mathbf{x}_i)\,.$$

and its mollified version:

$$\mathbf{F}^H_\varepsilon(\mathbf{x}) = -\sum_{i=1}^N \frac{2\mu+\lambda}{\mu}\pi a_i^2\overline{p}_i\,\nabla\delta^\varepsilon(\mathbf{x}-\mathbf{x}_i)\,.$$

In the two dimensional model, one can use either $\mathbf{F}^S_a$, $\mathbf{F}^S_\varepsilon$, or $\mathbf{F}^H_\varepsilon$ as forcing terms and obtain a solution that approximates the exact solution outside of the vessels up to higher order terms with respect to both the ratio a/R and ε.

When considering finite dimensional approximations, the first two choices require the full discretization of the vessel boundary Γ or of the fictitious boundary ∂B_ε, while employing $\mathbf{F}^H_\varepsilon$ only requires evaluation of the integrals expressed in Equation (20).

3 Three-dimensional case

In three dimensions, we consider each vessel as a thin cylindrical domain, described via a one-dimensional manifold, denoted as the *centerline*, and a radius varying along the centerline. In order

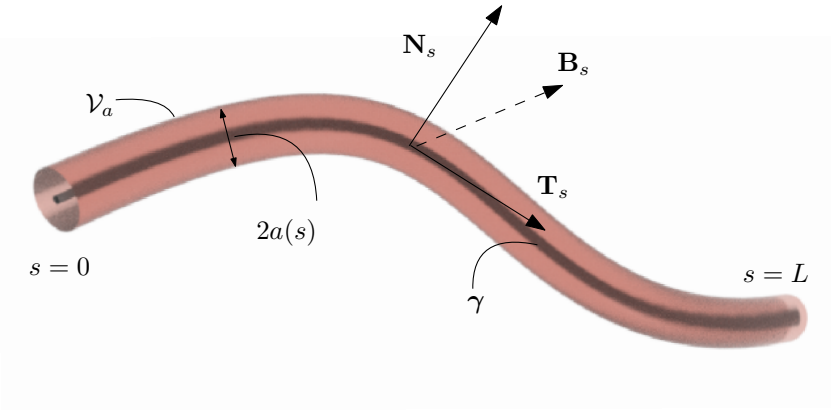

Figure 5: Sketch of a 3D vessel, identified via its cross-sectional radius and its centerline.

to obtain the singular source terms, we will then integrate over the centerline the equivalent of the two-dimensional formulation discussed in Section 2 considered on a plane that is locally orthogonal to the centerline.

In what follows, we will also assume that curvature of the vessels varies slowly w.r.t. to its arclength, so that its effect, as well as elastic effects of the vessels, may be neglected. For a possible way to include the elastic behaviour of the vessels we refer to [2]. In each cross sectional plane of the vessel, we approximate the local behaviour of the problem as in the two-dimensional axi-symmetric case.

3.1 Geometrical setting

Let us introduce a one-dimensional arc-length curve

$$\boldsymbol{\gamma}(s) : [0, L] \to \Omega \subset R^3,$$

describing the vessel centerline, and a positive function

$$a(s) : [0, L] \to \Omega \subset R,$$

standing for the radius of the cross-section at each $s \in [0, L]$. Moreover, let us denote with $A(s)$ the cross-section, i.e., the disk of radius $a(s)$ orthogonal to $\boldsymbol{\gamma}(s)$, and with $|A(s)|$ the cross-sectional area, for all $s \in [0, L]$ (see Figure 5).

In order to formally derive the multiscale model, we introduce at each $s \in [0, L]$ also the *Frenet* frame $\mathbf{T}_s = c'(s)$ (tangential vector in s), $\mathbf{N}_s = \mathbf{T}'_s/|\mathbf{T}'_s|, \mathbf{B}_s = \mathbf{T}_s \times \mathbf{N}_s$ (basis of the normal plane in s).

Finally, we assume that the fluid pressure within the vessel is constant over each cross section, thus introducing a function

$$p_{\boldsymbol{\gamma}}(s) : [0, L] \to \Omega \subset R,$$

denoting the excess pressure along the centerline.

Let us consider a three-dimensional domain Ω, the set

$$\mathcal{V}_a(\boldsymbol{\gamma}) = \{\mathbf{x} \in \Omega \text{ s.t. } \mathrm{dist}(\mathbf{x}, \boldsymbol{\gamma}) < a\}, \tag{22}$$

(denoting the vessel domain) and the tissue domain $\Omega_a = \Omega \backslash \mathcal{V}_a$. Moreover, let $\Gamma = \partial \mathcal{V}_a(\boldsymbol{\gamma})$.

We assume that the domain $\mathcal{V}_a(\boldsymbol{\gamma})$ is non-intersecting, i.e., the coordinate transformation mapping

$$\boldsymbol{\varphi}(r,\theta,s) := \boldsymbol{\gamma}(s) + r\cos(\theta)\mathbf{N}_s + r\sin(\theta)\mathbf{B}_s, \tag{23}$$

is one-to-one from $(r,\theta,s) \in (0,a(s)] \times [0,2\pi] \times [0,L]$ to $\mathcal{V}_a(\boldsymbol{\gamma})$.

We denote with $\gamma^{-1} : \mathcal{V}_a(\boldsymbol{\gamma}) \mapsto [0,L]$ the function that identifies, for each point $\mathbf{x}$ in $\mathcal{V}_a(\boldsymbol{\gamma})$, the arc-length coordinate $s \in [0,L]$ such that $\boldsymbol{\gamma}(s)$ has minimum distance from $\mathbf{x}$, i.e.,

$$\gamma^{-1}(\boldsymbol{\varphi}(r,\theta,s)) := s, \qquad \forall r \in [0,a(s)], \quad \forall \theta \in [0,2\pi]. \tag{24}$$

Assuming that the pressure is constant over cross-sections, we define an extension p (defined in the three dimensional vessel) of the one-dimensional excess pressure $p_{\boldsymbol{\gamma}}$ via

$$p(\mathbf{x}) = p_{\boldsymbol{\gamma}}\left(\gamma^{-1}(\mathbf{x})\right) \,, \forall \mathbf{x} \in \mathcal{V}_a \,.$$

3.2 The singular formulation

As in the previous case, we aim to solve an elasticity problem on the domain Ω_a by constructing variational formulation on the whole three-dimensional domain Ω, in which the elasticity problem in Ω_a is extended by a fictitious problem in $\mathcal{V}_a$. Proceeding analogously as in Section 2.3, we seek for the solution of a problem of the form

Problem 3.1 (3D, variational) *Given the excess pressure field $p_{\boldsymbol{\gamma}}$, the vessel configuration $\boldsymbol{\gamma}$, and the radius function a, find $\mathbf{u} \in V$ such that*

$$(2\mu e(\mathbf{u}), e(\mathbf{v}))_\Omega + (\lambda \operatorname{div}\mathbf{u}, \operatorname{div}\mathbf{v})_\Omega = < \mathbf{F}_{(\boldsymbol{\gamma},p_{\boldsymbol{\gamma}},a)}, \mathbf{v} > \quad \forall \mathbf{v} \in V.$$

The source term $\mathbf{F}_{(\boldsymbol{\gamma},p_{\boldsymbol{\gamma}},a)}$ shall be defined in such a way to enforce, for each $s \in [0,L]$, a given jump of the normal stresses across $\Gamma \cap A(s)$.

Ideally, we would like to use the same reasoning that lead to the definition of the two-dimensional model problem, that is, defining $\mathbf{F}_{(\boldsymbol{\gamma},p_{\boldsymbol{\gamma}},a)}$ such that the solution $\mathbf{u}$ coincides with the one that would be obtained by solving the true problem in the elastic matrix alone, with non-homogemous Neumann boundary conditions on the vessel boundary Γ depending on the pressure $p_{\boldsymbol{\gamma}}$.

However, in three dimensions, an explicit solution is only available for trivial vessel geometries and boundary conditions, unless we assume that all quantities that change along the vessel coordinate direction varies slowly w.r.t. to s. In this case we could still use the same principle used in the two dimensional approximation by integrating the derivation of the two-dimensional model problem along the arclength s. We start by constructing a force distribution $\mathbf{F}^S(\boldsymbol{\gamma}, p_{\boldsymbol{\gamma}}, a)$ given by

$$\begin{aligned} < \mathbf{F}^S_{(\boldsymbol{\gamma},p_{\boldsymbol{\gamma}},a)}, \mathbf{v} > &:= \int_\Gamma \frac{(2\mu+\lambda)}{\mu} p(\mathbf{y})\,\mathbf{n}(\mathbf{y}) \cdot \mathbf{v}(\mathbf{y})\,\mathrm{d}\Gamma_{\mathbf{y}} \\ &= \int_\Gamma \frac{(2\mu+\lambda)}{\mu} p(\mathbf{y})\,\mathbf{n}(\mathbf{y}) \cdot \int_\Omega \mathbf{v}(\mathbf{x})\delta(\mathbf{x}-\mathbf{y})\,\mathrm{d}\mathbf{x}\,\mathrm{d}\Gamma_{\mathbf{y}} \\ &= \int_\Omega \mathbf{v}(\mathbf{x}) \cdot \left(\int_\Gamma \frac{(2\mu+\lambda)}{\mu} p(\mathbf{y})\,\mathbf{n}(\mathbf{y})\delta(\mathbf{x}-\mathbf{y})\,\mathrm{d}\Gamma_{\mathbf{y}} \right) \mathrm{d}\mathbf{x}\,. \end{aligned} \tag{25}$$

In 3D, it is therefore possible to define the singular source term as an integral over the vessel boundary of the form

$$\mathbf{F}^S_{(\boldsymbol{\gamma},p_{\boldsymbol{\gamma}},a)}(\mathbf{x}) := \int_\Gamma \frac{(2\mu+\lambda)}{\mu} p(\mathbf{y})\,\mathbf{n}(\mathbf{y})\delta(\mathbf{x}-\mathbf{y})\,\mathrm{d}\Gamma_{\mathbf{y}},\ \forall \mathbf{x}\in\Omega\,.$$

The next step is to generalize the singular formulation in order to impose a given jump of the normal stresses across the boundary of a vessel defined by the centerline $\boldsymbol{\gamma}([0,L])$ and an arbitrary, constant, radius $\varepsilon > 0$. Let $\mathcal{V}_\varepsilon(\boldsymbol{\gamma})$ denote the generalized vessel of radius ε, defined analogously to $\mathcal{V}_a(\boldsymbol{\gamma})$ in (22), and let $\Gamma^\varepsilon = \partial V_\varepsilon(\boldsymbol{\gamma})$ represent the boundary of such generalized vessel.

Proceeding as in the two-dimensional case, we introduce

$$\hat{g}_a(s) := \pi a^2(s) p_{\boldsymbol{\gamma}}(s)\frac{(2\mu+\lambda)}{\mu}. \tag{26}$$

which is based on the approximation of the jump across the vessel boundary in the two-dimensional case (see (21)), and the forcing term

$$\mathbf{F}^S_{(\boldsymbol{\gamma},p_{\boldsymbol{\gamma}},\varepsilon)}(\mathbf{x}) := \int_{\Gamma^\varepsilon} \frac{\hat{g}_a(\gamma^{-1}(\mathbf{y}))}{\pi\varepsilon^2}\,\mathbf{n}(\mathbf{y})\delta(\mathbf{x}-\mathbf{y})\,\mathrm{d}\Gamma_{\mathbf{y}},\ \forall \mathbf{x}\in\Omega\,. \tag{27}$$

3.3 The hyper-singular formulation

Let us introduce the extension of $\hat{g}_a$ on $\mathcal{V}_\varepsilon(\boldsymbol{\gamma})$ defined by

$$\hat{g} := \hat{g}_a \circ \gamma^{-1} \tag{28}$$

and consider, for any function $\mathbf{v} \in (C^1(\Omega))^3$ the limit

$$\begin{aligned}
\lim_{\varepsilon\to 0} < \mathbf{F}^S_{(\boldsymbol{\gamma},p_{\boldsymbol{\gamma}},\varepsilon)}, \mathbf{v} > &= \lim_{\varepsilon\to 0} \int_{\Gamma^\varepsilon} \frac{\hat{g}}{\pi\varepsilon^2}\mathbf{v}\cdot\mathbf{n}\,\mathrm{d}\Gamma_{\mathbf{x}} \\
&= \lim_{\varepsilon\to 0} \int_{\mathcal{V}_\varepsilon(\boldsymbol{\gamma})} \frac{1}{\pi\varepsilon^2}\,\mathrm{div}\,(\hat{g}\mathbf{v})\,\mathrm{d}\mathbf{x} \\
&= \lim_{\varepsilon\to 0} \int_0^L \int_0^{2\pi} \int_0^\varepsilon \frac{1}{\pi\varepsilon^2}\,\mathrm{div}\,(\hat{g}\mathbf{v})\,\mathrm{d}r\,r\,\mathrm{d}\theta\,\mathrm{d}s \\
&= \int_0^L (\mathrm{div}\,(\hat{g}\mathbf{v}))\circ\boldsymbol{\gamma}\,\mathrm{d}s \\
&= \int_0^L (\mathbf{T}_s\hat{g}_a'\mathbf{v} + \hat{g}_a\,((\mathrm{div}\,\mathbf{v})\circ\boldsymbol{\gamma}))\,\mathrm{d}s \qquad \forall \mathbf{v}\in(C^1(\Omega))^3,
\end{aligned} \tag{29}$$

where we have used the identity $\nabla\hat{g} = (\mathbf{T}_s\hat{g}_a')\circ\gamma^{-1}$.

In view of (29), we consider the variational formulation

$$(2\mu e(\mathbf{u}), e(\mathbf{v}))_\Omega + (\lambda\,\mathrm{div}\,\mathbf{u}, \mathrm{div}\,\mathbf{v})_\Omega = < \mathbf{F}^H_{(\boldsymbol{\gamma},p_{\boldsymbol{\gamma}},a)} + \mathbf{F}^T_{(\boldsymbol{\gamma},p_{\boldsymbol{\gamma}},a)}, \mathbf{v} > \quad \forall \mathbf{v}\in C^1(\Omega)$$

where the right hand side can be defined through the hyper-singular term

$$\mathbf{F}^H_{(\boldsymbol{\gamma},p_{\boldsymbol{\gamma}},a)}(\mathbf{x}) := -\int_0^L \hat{g}_a(s)\nabla\delta(\mathbf{x}-\boldsymbol{\gamma}(s))\,\mathrm{d}s, \qquad \forall \mathbf{x}\in\Omega\,. \tag{30}$$

and the singular source

$$\mathbf{F}^T_{(\boldsymbol{\gamma},p_{\boldsymbol{\gamma}},a)}(\mathbf{x}) = \int_0^L \hat{g}'_a(s)\mathbf{T}_s\,\delta(\mathbf{x}-\boldsymbol{\gamma}(s))\,\mathrm{d}s, \qquad \forall \mathbf{x}\in\Omega\,. \tag{31}$$

which has support on the centerline and it is directed tangential to it.

Remark 3.1 *Notice that the force introduced in* (30)-(31) *depends only on one-dimensional information, such as centerline, the excess pressure $p(s)$, the radius, and the cross-sectional area, and it allows therefore to represent the vessel uniquely through a one-dimensional manifold.*

Remark 3.2 *Similarly to what happens in the two-dimensional case, the forcing term given in Equation* (29) *is not in V^*, and we should replace $\mathbf{F}^S_{\boldsymbol{\gamma}}$ with a mollified version $\mathbf{F}^S_{(\boldsymbol{\gamma},p_{\boldsymbol{\gamma}},a),\epsilon}$ where the Dirac delta distribution δ is replaced by a regularized version of it, δ^ε, depending on a resolution parameter ε.*

4 The discrete problem

Let us now assume to deal with a polygonal or polyhedral domain Ω, and let $\{\mathcal{T}_h\}_h$ be a family of conformal, quasi-uniform quadrilateral or hexaedral meshes exactly covering Ω where h denotes the maximum element diameter.

We construct the finite element space of globally continuous piecewise polynomials of order k in each coordinate directions defined by:

$$V_h := \{\mathbf{v} \in (H^1_{\Gamma_D}(\Omega))^d, \text{ s.t. } \mathbf{v}|_T \in \mathcal{Q}^k(T) \ \forall T \in \mathcal{T}_h, \mathbf{v}|_{\Gamma_D} = 0\}, \tag{32}$$

denoting with m its dimension and with $\{\hat{\mathbf{v}}_i\}_{i=1}^m$ a basis for the space.

We consider the following discrete problem:

Problem 4.1 (3D, Discrete) *Let be given a curve $\boldsymbol{\gamma} : [0,L] \to \mathbb{R}^3$, a function $a : [0,L] \to \mathbb{R}$ describing the radius, and a pressure $p_{\boldsymbol{\gamma}} : [0,L] \to \mathbb{R}$. Moreover, let $\boldsymbol{F}$ be one of the singular or hyper-singular source terms defined in the previous sections. Find the displacement $\mathbf{u}_h \in V_h$ such that*

$$(2\mu e(\mathbf{u}_h), e(\mathbf{v}_h))_\Omega + (\lambda\nabla\cdot\mathbf{u}_h, \operatorname{div}\mathbf{v}_h)_\Omega = <\boldsymbol{F}, \mathbf{v}_h>, \qquad \forall \mathbf{v}_h \in V_h. \tag{33}$$

Problem 4.1 reduces to the solution of the following linear system of equations

$$\boldsymbol{K}\boldsymbol{U} = \boldsymbol{b}, \tag{34}$$

where

$$\begin{aligned} \boldsymbol{K}_{ij} &:= 2\mu(e(\hat{\mathbf{v}}_j), e(\hat{\mathbf{v}}_i))_\Omega + \lambda(\nabla\cdot\hat{\mathbf{v}}_j, \operatorname{div}\hat{\mathbf{v}}_i)_\Omega \\ \boldsymbol{b}_i &:= <\boldsymbol{F}, \hat{\mathbf{v}}_i>_\Omega, \end{aligned} \tag{35}$$

and $\boldsymbol{U} = \{u^i\}_{i=1,\dots,m}$ indicates the vector of coefficients of the finite element function $\mathbf{u}_h$ such that

$$\boldsymbol{u}_h(\mathbf{x}) = \sum_{i=1}^m u^i \mathbf{v}_i(\mathbf{x}) \quad \mathbf{x}\in\Omega. \tag{36}$$

The right-hand side of equation (33) contains a singular forcing term, whose numerical computation may require a discrete approximation of the Dirac delta distribution. We use one of the classical approximations widely employed in the context of the Immersed Boundary Method [27], i.e.,

$$\delta^\varepsilon(\mathbf{x}) := \frac{1}{\varepsilon^d} \prod_{i=1}^{d} \theta\left(\frac{\mathbf{x}_i}{\varepsilon}\right) \tag{37}$$

with

$$\theta(y) := \begin{cases} (\cos(\pi y) + 1)/2 & \text{if } -1 < y < 1 \\ 0 & \text{otherwise} \end{cases} \tag{38}$$

where ε is an arbitrary (small) parameter. In the numerical experiments presented in the following Section, we set $\varepsilon = 2h$, i.e., twice the diameter of the smallest triangulation element.

This approximation of the Dirac distribution guarantees that $\int_{\Re^d} \delta^\varepsilon \, \mathrm{d}\mathbf{x} = 1$ and that $\delta^\varepsilon \in C^1(\Re^d)$, making it a good candidate for a regularization of the Dirac distribution required for the hyper-singular formulation. For a in-depth discussion on alternative approximations of the Dirac distribution and of their approximation properties, we point the reader to the excellent work of [21].

5 Numerical results

This section is dedicated to the numerical validation of the mathematical models derived in Sections 2 and 3. We will consider first the simple 2D axi-symmetric situation with known exact solution. Next, we will investigate the effect of random distribution of vessels (in two and three dimensions) and use the hyper-singular formulation to derive a statistical model for the effective tissue behavior.

All numerical examples provided in this section were obtained using an open source code based on the `deal.II` library [4, 3, 1]. The code is freely available at the address `https://gitlab.com/code_projects/immersed-elasticity` ([14]), and it is inspired by the `deal.II` *step-60* tutorial [13]. All simulations were performed using $\mathcal{Q}^1$ conforming finite element spaces on quadrilaterals or hexaedral meshes.

5.1 Reference solution in two-dimension

We consider first a 2D axi-symmetric problem, comparing the results obtained via the proposed method employing three different source terms to approximate the vessel network:

(S) A singular forcing term, whose distributional definition is given by

$$< \boldsymbol{F}, \mathbf{v} >:= \int_{\Gamma^a} \frac{(2\mu + \lambda)}{\mu} p\mathbf{v} \, \mathrm{d}\Gamma$$

(RS) A regularized singular forcing term, given by

$$\boldsymbol{F}^\varepsilon(\mathbf{x}) := \int_{\Gamma^a} \frac{(2\mu + \lambda)}{\mu} p\delta^\varepsilon(\mathbf{x} - \mathbf{y}) \, \mathrm{d}\Gamma_y$$

(RHs) A regularized hyper-singular forcing term, given by

$$\boldsymbol{F}^\varepsilon(\mathbf{x}) := -\frac{(2\mu + \lambda)}{\mu} \pi a^2 p \nabla\delta^\varepsilon(\mathbf{x})$$

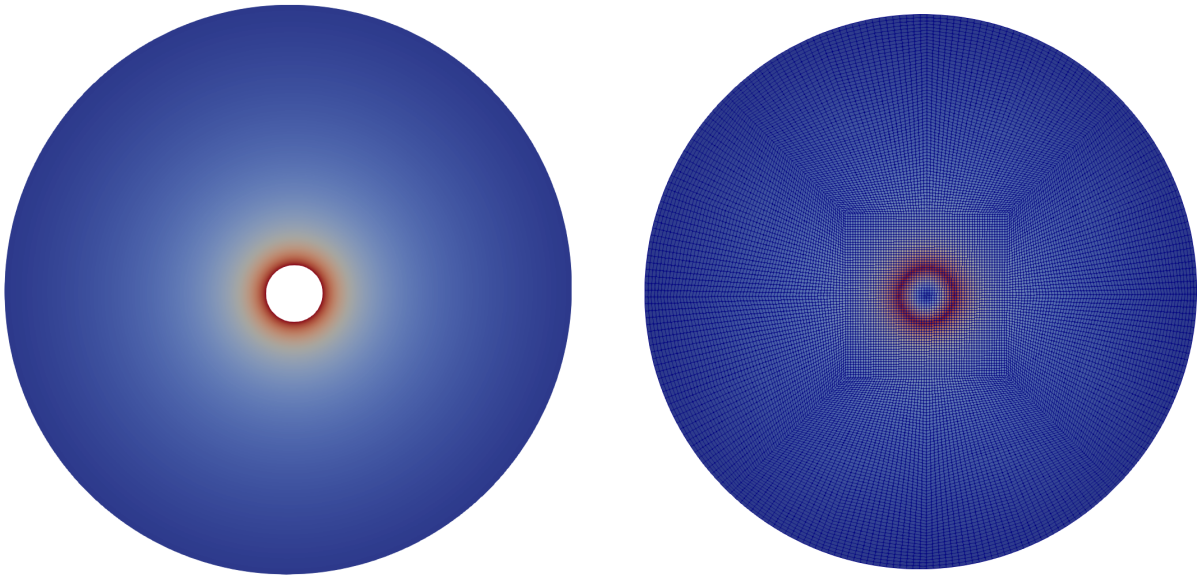

Figure 6: 2D axi-symmetric problem. Comparison between the exact solution (left) and the numerical solution obtained with the singular forcing term (case (S)).

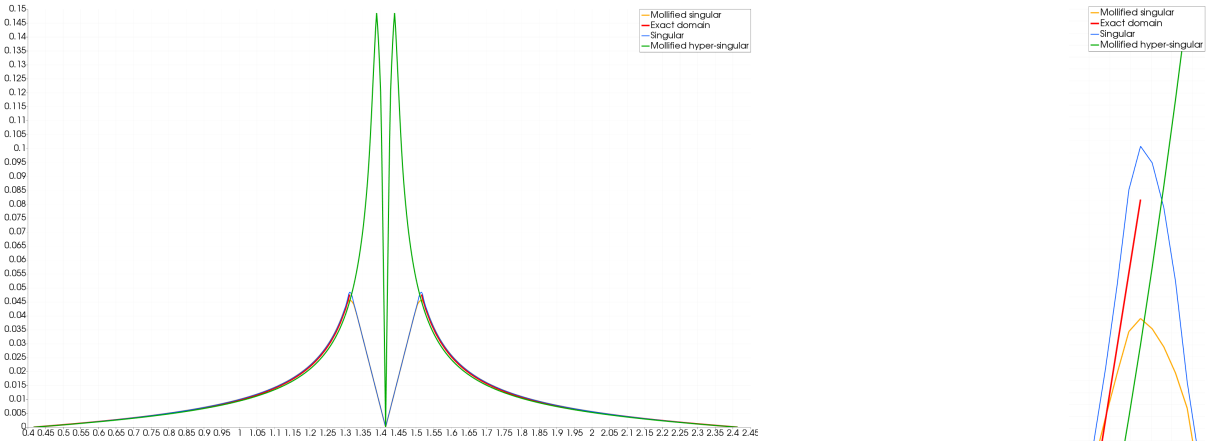

Figure 7: Comparison of displacement magnitude on a diagonal cut of the disk, between solution on exact domain, and the three different options for the right hand side term.

We consider $\lambda = \mu = p = 1$ Pa. Figure 6 shows the comparison, on a circular domain of radius $R = 1$, with a vessel of radius $a = .1$, between the exact solution (left plot) and the solution obtained using the singular source (S) (right plot).

Notice that the grid does not need to be aligned to the surface Γ, thanks to the non-matching interpolation techniques developed in [28, 16, 8, 12].

A more quantitative comparison is provided in Figure 7, showing the exact solution and the numerical solutions for the three different singular source definitions along along a diagonal cut of the domain. Although the ratio $\frac{a}{R}$ is not too small (equal to 0.1), the solutions are remarkably close outside of the vessel, in agreement with the asymptotic expansion (21), which predicts a residual error of the order of $\sim \mathcal{O}\big((a/R)^2\big)$.

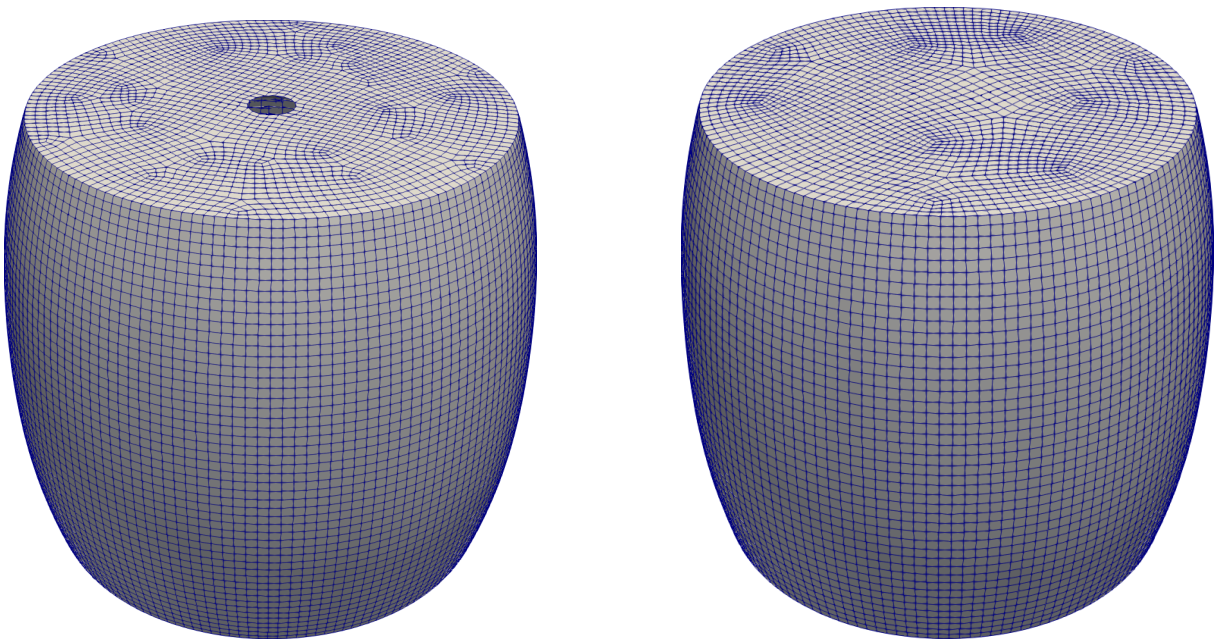

Figure 8: 3D axi-symmetric problem. Comparison between the numerical solution on the exact domain (left) and the numerical solution obtained with the regularized hyper-singular forcing term. The displacement has been amplified of a factor 20, to better appreciate the comparison.

5.2 Axi-symmetric test in three-dimension

As an extension of the simple two-dimensional axysymmetric case, we consider a three-dimensional extrusion of the two-dimensional case, where we probe the behaviour of our model with mixed boundary conditions.

We consider an elastic cylinder, clamped at the top and at the bottom, and stress free on the lateral surfaces, with a pressurised vessel in its center, and compare the result obtained using the exact domain, and a regularized hyper-singular forcing term (30), used to simulate the presence of the vessel:

$$\boldsymbol{F}^{\varepsilon}(\mathbf{x}) := -\int_{\Gamma} \frac{(2\mu+\lambda)}{\mu} \pi a^2 p \nabla \delta^{\varepsilon}(\mathbf{x}).$$

We consider $\lambda = \mu = p = 1$ Pa. Figure 8 shows the comparison, on a cylindrical domain of radius $R = 1$, height $H = 2$, with a vessel of radius $a = .1$, between the numerical solution on the exact domain (left plot) and the solution obtained using the hyper-singular source term (right plot).

The difference between the maximum displacement on the external boundary of the two domain is on the order of 10^{-4}, with a maximum displacement on the order of 10^{-2}, in agreement with the estimates on the ratio between R and a.

5.3 Curvature test in three-dimension

The next test is designed to understand the effect of the curvature of the vessel on our approximation, i.e., how strictly we should adhere to the requirements of small curvature. To this aim, we consider a quarter of a toroidal elastic domain, with a vessel in its center, fixed at the clipping regions. The vessel is pressurised at a given pressure.

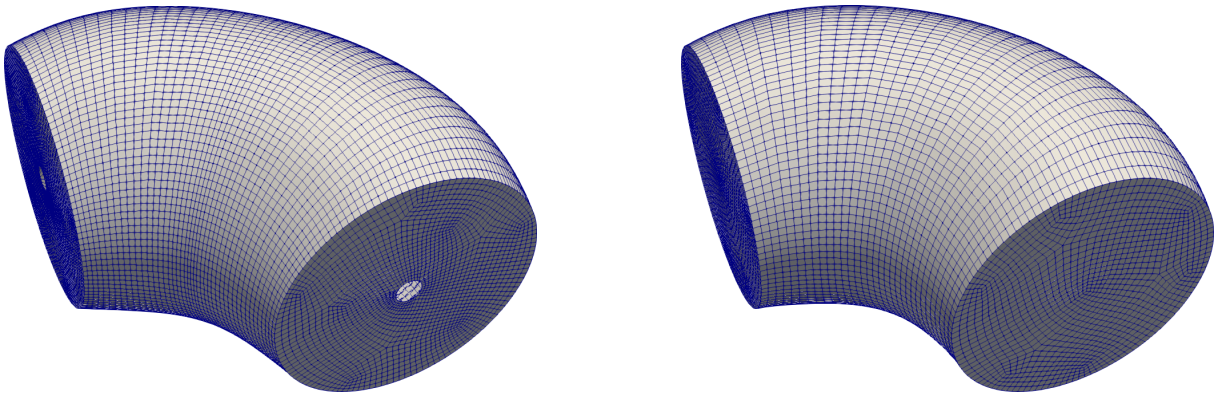

Figure 9: 3D toroidal problem. Comparison between the numerical solution on the exact domain (left) and the numerical solution obtained with the regularized hyper-singular forcing term. The displacement has been amplified of a factor 20, to better appreciate the comparison.

As in the previous test, we compare the result obtained using the exact domain, and a regularized hyper-singular forcing term (30).

We consider $\lambda = \mu = p = 1$ Pa. Figure 9 shows the comparison, on a quarter of a toroidal domain with major radius $R = 2$, minor radius $r = 1$, with a vessel of radius $a = .1$, between the exact solution (left plot) and the solution obtained using the singular source (right plot).

The difference between the maximum displacement on the external boundary of the two domain is on the order of 10^{-3}, with a maximum displacement on the order of 10^{-2}. In this case we can observe a deterioration in the solution of one order of magnitude, with respect to the model problem with no curvatre, suggesting that a better model may be devised for those cases where the curvature of the vessels may be significant.

5.4 In silico characterization of pressurised tissues

In the context of elastography, where data resolution (i.e., MRI images and acquired displacements) is typically much coarser than vessel diameter, it is interesting to derive an effective material of the biphasic tissue under consideration, i.e., to understand how the microscopic vasculature influences the mechanical parameters (Lamé coefficients) on a coarser level.

Let us consider the case of a thick tissue sample, subjected to a known deformation along a specified plane, such that strains along the orthogonal direction to the plane can be neglected. Such situation is commonly referred to as *plain-strain* case. Typical experimental settings – targeted to the quantification of elastic parameters – are designed to induce one of two ideal deformations: *pure shear* and *pure compression*, represented in Figure 10.

These experiments correspond to an essentially two-dimensional configuration where the displacements are given by, respectively, $\mathbf{u}_s = c(y, 0, 0)$ and $\mathbf{u}_d = \frac{c}{2}(x, y, 0)$, where c is an arbitrary constant. In these cases, it is easy to show that the corresponding stresses are given by

$$\sigma(\mathbf{u}_s) = c \begin{pmatrix} 0 & \mu & 0 \\ \mu & 0 & 0 \\ 0 & 0 & 0 \end{pmatrix} \qquad \sigma(\mathbf{u}_d) = c \begin{pmatrix} (\lambda+\mu) & 0 & 0 \\ 0 & (\lambda+\mu) & 0 \\ 0 & 0 & 0 \end{pmatrix}. \tag{39}$$

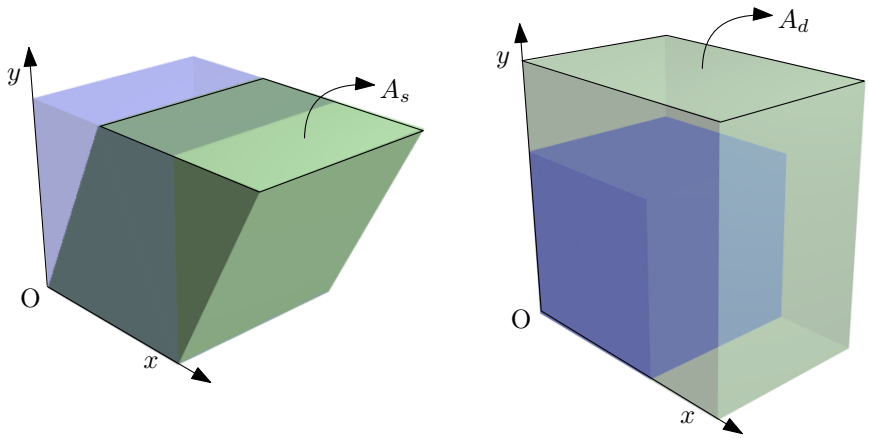

Figure 10: Typical plane strain experiments to infer μ and λ. Pure shear (left) and pure dilation (right).

By measuring the quantities

$$\begin{aligned} F_s &:= \int_{A_s} \sigma(\mathbf{u}_s) \cdot \mathbf{n} \, \mathrm{d}\partial\Omega = c|A_s|\mu \boldsymbol{e}_x \\ F_d &:= \int_{A_d} \sigma(\mathbf{u}_d) \cdot \mathbf{n} \, \mathrm{d}\partial\Omega = c|A_s|(\lambda+\mu)\mathbf{n}, \end{aligned} \tag{40}$$

it is thus possible to estimate μ and λ with two consecutive experiments (either imposing a force, and measuring the shear and/or the dilation, or viceversa). A two dimensional simulation in these cases is capable of capturing all the features of the problem.

However, when the tissue contains pressurized fluid vessels, it is no longer reasonable to assume that the stresses are the ones presented in equation 39. In this situation, the multiscale model introduced in Sections 2 and 3 allow for an efficient in silico characterization of the effective material properties.

In fact, let us consider a tissue domain Ω with a given distribution of vessels (e.g., recovered from imaging or generated artificially using statistical methods), and let β represents the volume fraction of Ω that is covered by vessels (e.g., for soft tissues, β is typically below 5%). Thanks to the structure of the immersed finite element method, we can additively decompose the solution, isolating the effect of the pressurized vessels on the right hand side. In other words, we can seek the solution $\mathbf{u}_h^p$ in V_h such that

$$(\sigma(\mathbf{u}_p^h), e(\mathbf{v}_h)) = (\boldsymbol{F}(p, a, \beta), \mathbf{v}_h)_\Omega \qquad \forall \mathbf{v}_h \in V_h. \tag{41}$$

5.4.1 Derivation in the uniform case

To begin with, let us consider the two-dimensional problem, with an uniform random spatial distribution of n random vessels located in $\{\mathbf{x}_i\}_{i=1}^n$, with radius a_i and with excess pressure p_i, for $i = 1, \dots, n$.

Let us now consider the Voronoi diagram covering the domain Ω with generators in $\{\mathbf{x}_i\}_{i=1}^n$ (as in Figure 11). Indicating with V_i the i-th Voronoi cell, and with $|V_i|$ its volume, we can define the local vessel density $\beta_i = \pi^2 a_i/|V_i|$, and we can interpret the forcing term in equation (41) as the

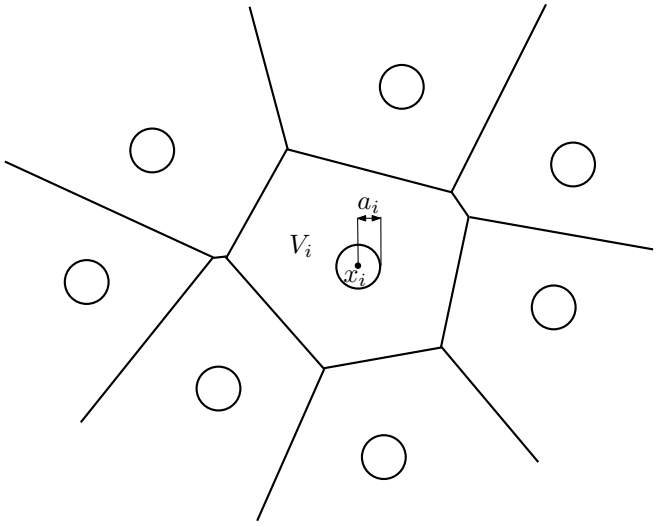

Figure 11: Voronoi diagram of the vessel centers for the two-dimensional case.

approximation through the Voronoi diagram of a *continuous* integral over the domain Ω:

$$\begin{aligned} < \boldsymbol{F}, \mathbf{v} > &:= \sum_{i=1}^{n} \frac{(2\mu+\lambda)}{\mu} p_i \pi a_i^2 \nabla \cdot \mathbf{v}(\mathbf{x}_i) = \sum_{i=1}^{n} |V_i| \frac{(2\mu+\lambda)}{\mu} p_i \frac{\pi a_i^2}{|V_i|} \nabla \cdot \mathbf{v}(\mathbf{x}_i) \\ &= \sum_{i=1}^{n} \beta_i |V_i| \frac{(2\mu+\lambda)}{\mu} p_i \nabla \cdot \mathbf{v}(\mathbf{x}_i) \\ &\simeq \sum_{i=1}^{n} \int_{V_i} \beta_i \frac{(2\mu+\lambda)}{\mu} p_i \nabla \cdot \mathbf{v}(\mathbf{x}) \simeq \int_{\Omega} \beta \frac{(2\mu+\lambda)}{\mu} p \nabla \cdot \mathbf{v} \, \mathrm{d}\Omega, \end{aligned} \tag{42}$$

where β and p are homogenised quantities that can vary spatially, and represent the local excess pressure and the local vessel density of the tissue.

This approximation yields an homogenized elasticity problem

$$(\sigma(\mathbf{u}_p^h), e(\mathbf{v}_h)) = \int_{\Omega} \beta \frac{(2\mu+\lambda)}{\mu} p \nabla \cdot \mathbf{v}_h \, \mathrm{d}\Omega \qquad \forall \mathbf{v}_h \in V_h, \tag{43}$$

where the forcing term on the right-hand-side acts on the dilatational part of the deformation. The solution to (43) satisfies the following conservation equation:

$$\int_{\Omega} 2\mu |e(\mathbf{u})|^2 + \lambda |\operatorname{div} \mathbf{u}|^2 \, \mathrm{d}\Omega = \int_{\Omega} \beta \frac{(2\mu+\lambda)}{\mu} p \nabla \cdot \mathbf{u} \, \mathrm{d}\Omega, \tag{44}$$

where one clearly sees that the pressurized vessel network acts as a non-conservative pressure source in the energy conservation equation.

If we consider homogenous Neumann boundary conditions, the force due to a uniform distribution of vessels, constant pressure and fixed volume fraction would produce – up to rigid deformations – a uniform dilation (or compression) in the form

$$\mathbf{u} = c\mathbf{x} \,. \tag{45}$$

Let d denote the dimension ($d = 2$ in the considered setting). In order to determine the constant c, we insert

$$|\operatorname{div} \mathbf{u}|^2 = c^2 d^2, \ |e(\mathbf{u})|^2 = c^2 d$$

into (44), obtaining

$$2\mu c^2 d + \lambda c^2 d^2 = \beta \frac{(2\mu+\lambda)}{\mu} pcd$$

and thus

$$c = \frac{\beta p}{\mu} \frac{2\mu+\lambda}{2\mu+\lambda d}. \tag{46}$$

The corresponding Cauchy stress is given by

$$\sigma(\mathbf{u}_p^h)\mathbf{n} = \frac{\beta p}{\mu}(2\mu+\lambda)\mathbf{n}, \tag{47}$$

and the corresponding total force $\mathbf{F}_p$ on the face A can be computed as

$$\mathbf{F}_p := \int_A \sigma(\mathbf{u}_p^h)\mathbf{n}\,\mathrm{d}A = |A|\frac{\beta p}{\mu}(2\mu+\lambda)\mathbf{n}. \tag{48}$$

In the case of a uniform spatial distribution of vessels, with constant vessel sizes and constant pressure, we obtain $(\mathbf{F}_p \cdot \mathbf{n})\mathbf{n} = \mathbf{F}$, i.e., the internal force generated by the pressurized vasculature is always directed along the normal direction to the surface.

Notice that the derivation of the total force (48) is based on the assumptions of Neumann boundary conditions and on the fact that the term $\beta\frac{(2\mu+\lambda)}{\mu}p$ is constant across the domain. In this situation, the divergence theorem yields

$$< \boldsymbol{F}, \mathbf{v} >= \int_\Omega \beta\frac{(2\mu+\lambda)}{\mu} p\nabla\cdot\mathbf{v}\,\mathrm{d}\Omega = \int_{\partial\Omega} \beta\frac{(2\mu+\lambda)}{\mu} p\mathbf{v}\cdot\mathbf{n}\,\mathrm{d}\Gamma. \tag{49}$$

The same argument cannot be used in the case of homogeneous Dirichlet boundary conditions. In fact, the term on the right-hand-side of Equation (49) would be tested against functions $\mathbf{v}$ in V, whose value on $\partial\Omega$ would be zero, meaning that a uniform distribution of vessels with constant pressure has no effect on the solution.

In reality, since the distribution of vessels is discrete (although uniform), its effect should be noticeable also with Dirichlet boundary conditions, by measuring $\mathbf{F}_p = \int_A \sigma(\mathbf{u}_p^h)\mathbf{n}$ for each of the faces of the domain. By linearity, this should be equal (on average) to Equation (48).

5.4.2 Two-dimensional case

In this section, we probe the hypothesis derived in Section 5.4.1 by performing a set of statistical simulations in two dimensions, in which we consider several realizations of a random collection of vessels in a box domain $\Omega = [0,1]^2$, we impose zero Dirichlet conditions, and we measure the effects of the deformations on the boundary, by averaging the forces exerted by the expanding solid on the faces.

In this set of tests, we fix $\mu = 1$, $p = 1$, and we vary λ, the number of vessels, the radius, and the refinement level of the grid, to understand the robustness of the method with respect to grid size, vessel density, and material properties. In the presented simulation, the grid size is given by $h = 2^{-\mathsf{ref}}$, where ref will be denoted as the refinement level.

The vessels are randomly distributed on Ω, assuring that they do not intersect the boundary. An example of resulting distribution, considering 500 randomly distributed vessels of radius 5.65×10^{-3}

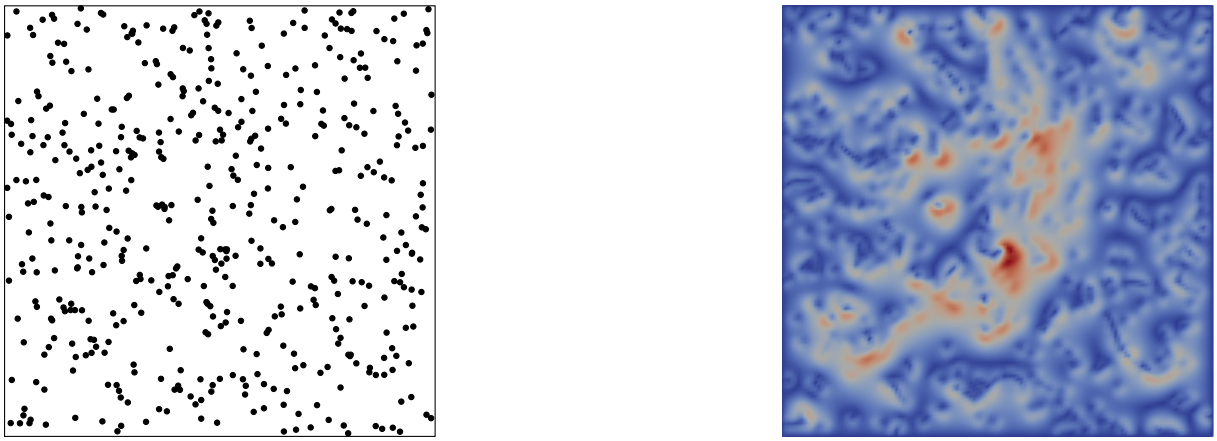

Figure 12: Left: Example of random realization with 500 vessels of radius 5.65×10^{-4} ($\beta = 5\%$). Displacement field, obtained with $\lambda = 1$ and mesh refinement level 7 ($h = 2^{-7} = 7.8125 \times 10^{-3}$, number of degrees of freedom equal to $33,282$). The maximum displacement is on the order of 10^{-3}.

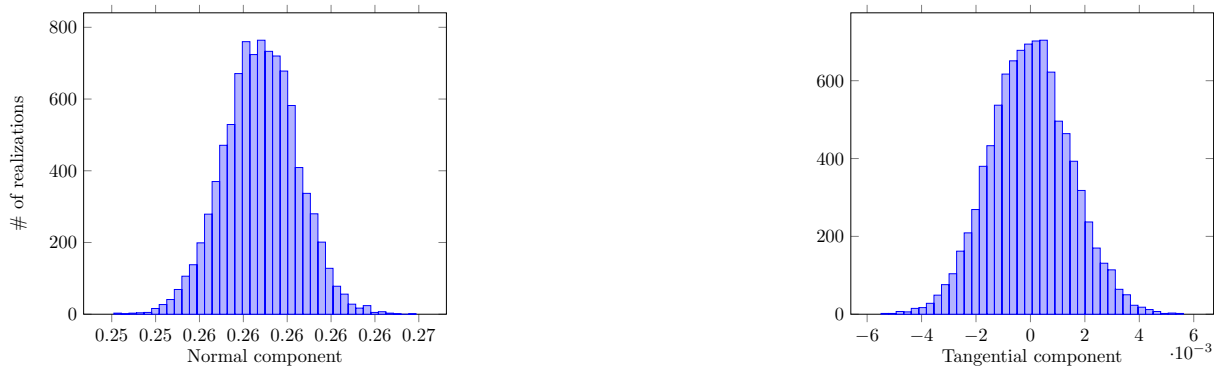

Figure 13: Statistical distribution of the normal (left) and tangential (right) pressure force, generated with $\beta \simeq 5\%$, $\lambda = 1$, $p = 1$, and refinement refinement level 9 on 10,000 realizations.

(total volume fraction $\beta \approx 0.05$) is provided in Figure 12 (left), while Figure 12 (right) shows the results obtained with $\lambda = 1$.

Figure 13 shows the statistical distribution of the normal and tangential pressure force for 10,000 realizations of randomly distributed vessels with fixed volume fraction $\beta \simeq 5\%$, Lamè parameter $\lambda = 1$, and constant pressure $p = 1$, on a grid with refinement refinement level 9 ($h = 2^{-9} = 1.953125 \times 10^{-3}$).

Figure 14 shows the mean normal force (with $\lambda = 1$ and $\lambda = 10$) as a function of the volume fraction β. The error bars show the value of the standard deviation, which are only visible in the plot for the refinement 8 case, as in the case with refinement 9 they are much smaller in scale.

5.4.3 Three dimensional case (aligned vessels)

In the three-dimensional setting, the homogenized hypothesis derived in Section 5.4.1 are more difficult to probe because vessels are anysotropic in nature, and realizations with totally random distributions of vessels would be unphysical, corresponding to point sources of excess pressure as opposed to “vessel sources”.

Figure 14: Mean and variance (vertical bars) value of the normal component of the force on the pressurized tissue computed from the statistical simulations, with refinement level 8 (left) and 9 (right), compared with the value estimated in (48), for $\lambda = 1$ (bottom three experimental measures) and $\lambda = 10$ (top three experimental measures).

For simpler settings, where the vessels are uniformly distributed and alligned along a preferred direction, the estimated forces of the two-dimensional case presented in Equation (48) are still a reasonable estimate of the force generated by the pressurised vessels measured on boundary walls whose normals are orthogonal to the vessels center-line, but cannot be used to estimate the forces on walls whose normal is parallel to the vessels. The two-dimensional setting corresponds to an infinite material along the z-direction, where deformation and stress are negligible along the z-direction.

In the finite-domain case, boundary effects become more and more important, and introduce a distortion in the homogenized estimate given by Equation (48). In this section we consider several realizations of random collection of streight vessels, aligned in the z-direction, included a box domain $\Omega = [0, 1]^3$, as depicted in Figure 15.

We impose zero Dirichlet conditions, and we measure the effect of the deformations on the boundary due to the pressurised vessels, by averaging the forces exerted by the expanding solid on the faces. By symmetry, the z-component of the total force on each lateral face is zero. In Figure 16, we show the statistical distribution of the non-zero components of the total force on the lateral faces of the cube.

For a domain that is infinitely long in the z-direction, this distribution should correspond to the estimates provided by the homogeneized expression of Equation (48). By constrast, the force exerted on the top and bottom faces is not taken into account by Equation (48). For an infinte domain, with Neumann boundary conditions on the lateral faces, this force should be zero. However, in this case we have a finite domain, and we impose Dirichlet boundary conditions. Figure 17 shows the statistical distribution of the normal and x-components on the top face of the domain.

6 Conclusions

We presented a multiscale modeling of biphasic tissues composed by an elastic matrix and a set of thin vessels. Our approach is based on neglecting long range interactions and treating the interface between solid and fluid as an immersed one dimensional manifold (described by centerline, radius, and pressure), taking into account the effect of the vascular network in terms of additional singular terms in the elasticity equations.

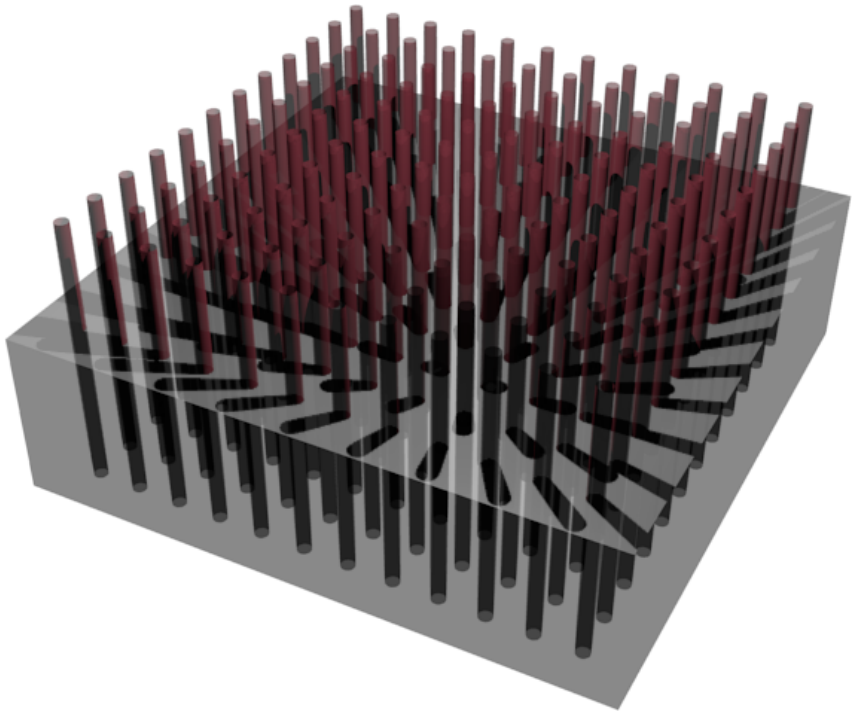

Figure 15: Schematic cut-view of a three-dimensional realization of a uniform distribution of vessels aligned along the z-axis.

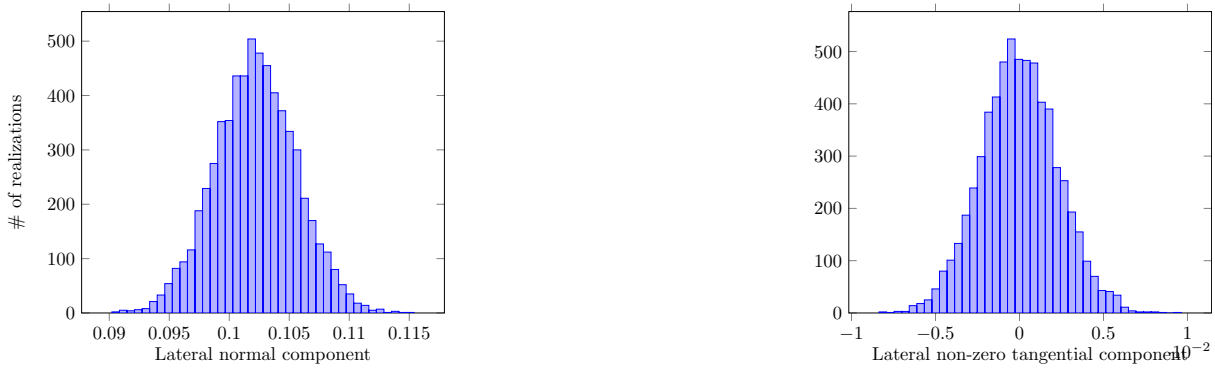

Figure 16: Statistical distribution of the lateral normal (left) and of the lateral non-zero tangential (right) pressure force, generated with $\beta \simeq 5\%$, $\lambda = 1$, $p = 1$, and refinement refinement level 6 on 6,000 realizations.

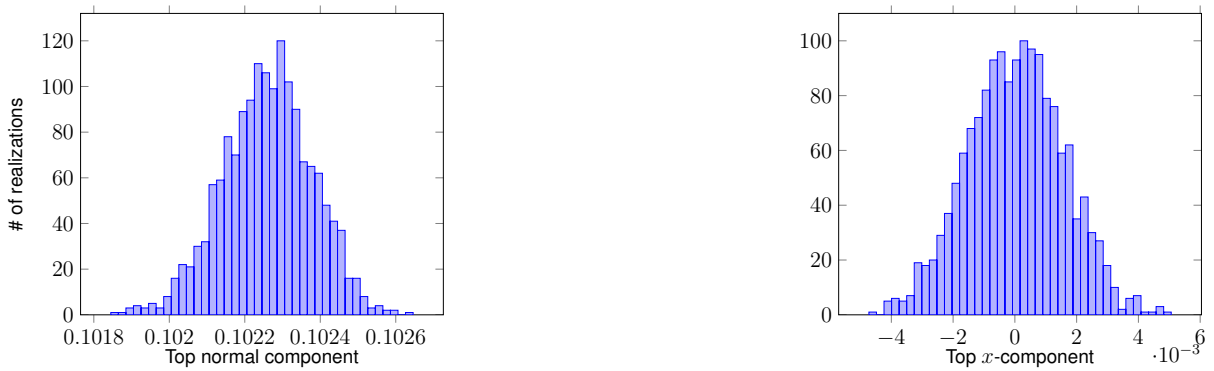

Figure 17: Statistical distribution of the top and bottom normal (left) and along the x-direction (right) pressure force, generated with $\beta \simeq 5\%$, $\lambda = 1$, $p = 1$, and refinement refinement level 6 on 1,500 realizations.

The main advantage of this method is that it reduces drastically the computational complexity when dealing with large networks of vessels, as it does not require to fully resolve the fluid-solid interface within the computational mesh.

We show different numerical tests, showing that the proposed reduced model yield a good qualitative agreement with the exact (when available) and fully resolved solutions, when considering a single vessel in two and three dimensional settings.

Moreover, we investigated the possibility of employing this multiscale model for the in silico characterization of the mechanical properties of a pressurized tissue. In this case, we showed first that the variational formulation with immersed singular terms can be used for deriving an effective tissue description (i.e., where the effect of pressurized vessels is upscaled into tissue properties) in the uniform case, i.e., when the vasculature can be approximated by an uniform vessel distribution. As next, we validated this hypothesis via a set of statistical simulations, in order to correlate effective material properties with the volume fraction of the vasculature and vessel pressure. The presented examples showed that the non-matching immersed method can be potentially used in order to investigate, in silico and from a statistical perspective, the mechanical behavior of the tissue given the (statistical) properties of the vasculature. To this respect, the main advantage of the immersed formulation is that the same computational mesh can be employed for simulating different realization, since the vessels are not explicitly resolved by the mesh. A detailed assessment of the proposed immersed method in the context of inverse problems in tissue mechanics is currently ongoing.

In this paper, we focused on the situation of a static fluid (at a given pressure) and of a linearly elastic solid. The generalization to more complex structural models (e.g., poroelasticity), as well as to the fluid-structure interaction case, i.e., where fluid pressure is affected by the surrounding matrix, are subject of current research.

References

[1] Alzetta, G., Arndt, D., Bangerth, W., Boddu, V., Brands, B., Davydov, D., Gassmöller, R., Heister, T., Heltai, L., Kormann, K., Kronbichler, M., Maier, M., Pelteret, J.P., Turcksin, B., Wells, D.: The deal.II Library, Version 9.0. Journal of Numerical Mathematics (2018)

[2] Alzetta, G., Heltai, L.: Multiscale modeling of fiber reinforced materials via non-matching im-

mersed method (2018). Submitted

[3] Arndt, D., Bangerth, W., Davydov, D., Heister, T., Heltai, L., Kronbichler, M., Maier, M., Pelteret, J.P., Turcksin, B., Wells, D.: The deal.II library, version 8.5. Journal of Numerical Mathematics **25**(3), 137–145 (2017)

[4] Bangerth, W., Hartmann, R., Kanschat, G.: deal.II—A general-purpose object-oriented finite element library. ACM Transactions on Mathematical Software **33**(4), 24–es (2007)

[5] Boffi, D., Gastaldi, L.: A finite element approach for the immersed boundary method. Computers & Structures **81**(8-11) (2003)

[6] Boffi, D., Gastaldi, L.: The immersed boundary method: a finite element approach. In: K. Bathe (ed.) Computational Fluid and Solid Mechanics 2003, vol. 2, pp. 1263–1266. Elsevier (2003)

[7] Boffi, D., Gastaldi, L., Heltai, L.: Numerical stability of the finite element immersed boundary method. Mathematical Models & Methods In Applied Sciences **17**(10), 1479–1505 (2007)

[8] Boffi, D., Gastaldi, L., Heltai, L., Peskin, C.S.: On the hyper-elastic formulation of the immersed boundary method. Computer Methods in Applied Mechanics and Engineering **197**(25-28), 2210–2231 (2008)

[9] Cattaneo, L., Zunino, P.: A computational model of drug delivery through microcirculation to compare different tumor treatments. International Journal for Numerical Methods in Biomedical Engineering **30**(11), 1347–1371 (2014)

[10] D'Angelo, C.: Finite element approximation of elliptic problems with Dirac measure terms in weighted wpaces: applications to one- and three-dimensional coupled problems. SIAM J. Numer. Anal. **50**(1), 194–215 (2012)

[11] D'Angelo, C., Quarteroni, A.: On the Coupling of 1D and 3D Diffusion-Reaction Equations. Application to Tissue Perfusion Problems. Math. Models Methods Appl. Sci. (M3AS) **18**(8), 1481–1504 (2008)

[12] Heltai, L.: On the stability of the finite element immersed boundary method. Computers & Structures **86**(7-8), 598–617 (2008)

[13] Heltai, L., Alzetta, G.: The deal.ii tutorial step-60: non-matching grid constraints through distributed lagrange multipliers (2018)

[14] Heltai, L., Caiazzo, A.: Immersed finite element elasticity method (2018)

[15] Heltai, L., Costanzo, F.: Variational implementation of immersed finite element methods. Computer Methods in Applied Mechanics and Engineering **229-232**(54/2011/M), 110–127 (2012)

[16] Heltai, L., Costanzo, F.: Variational implementation of immersed finite element methods. Computer Methods in Applied Mechanics and Engineering **229–232**(0), 110 – 127 (2012)

[17] Heltai, L., Rotundo, N.: Error estimates in weighted sobolev norms for finite element immersed interface methods. Tech. rep., WIAS (2016)

[18] Hirsch, S., Beyer, F., Guo, J., Papazoglou, S., Tzschaetzsch, H., Braun, J., Sack, I.: Compression-sensitive magnetic resonance elastography. Physics in Medicine and Biology **58**(15), 5287–5299 (2013)

[19] Hirsch, S., Guo, J., Reiter, R., Schott, E., Büning, C., Somasundaram, R., Braun, J., Sack, I., Kroencke, T.: Towards compression-sensitive magnetic resonance elastography of the liver: sensitivity of harmonic volumetric strain to portal hypertension. J Magn Reson Imaging **39**(2), 298–306 (2014)

[20] Hirsch, S., Sack, I., Braun, J.: Magnetic resonance elastography: physical background and medical applications. John Wiley & Sons (2017)

[21] Hosseini, B., Nigam, N., Stockie, J.M.: On regularizations of the Dirac delta distribution. Journal of Computational Physics **305**, 423–447 (2016)

[22] Mittal, R., Iaccarino, G.: Immersed boundary methods. Annual Review of Fluid Mechanics **37**(1), 239–261 (2005)

[23] Müller, L.O., Blanco, P.J., Watanabe, S.M., , Feijóo, R.A.: A high-order local time stepping finite volume solver for one-dimensional blood flow simulations: application to the ADAN model. Int. J. Numer. Meth. Biomed. Engng. **32**(10), e02,761 (2016). (in press)

[24] Muthupillai, R., Ehman, R.L.: Magnetic resonance elastography. Nat. Med. **2**, 601–603 (1996)

[25] Peskin, C.S.: Flow patterns around heart valves: A numerical method. Journal of Computational Physics **10**(2), 252–271 (1972)

[26] Peskin, C.S.: The immersed boundary method. Acta Numerica **11**(1), 479–517 (2002)

[27] Peskin, C.S.: The immersed boundary method. Acta Numerica **11**(1), 479–517 (2002)

[28] Roy, S., Heltai, L., Costanzo, F.: Benchmarking the immersed finite element method for fluid-structure interaction problems. Computers and Mathematics with Applications **69**, 1167–1188 (2015)

[29] Sack, I., Beierbach, B., Hamhaber, U., Klatt, D., Braun, J.: Non-invasive measurement of brain viscoelasticity using magnetic resonance elastography. NMR Biomed. **21**(3), 265–271 (2008)

[30] Wuerfel, J., Paul, F., Beierbach, B., Hamhaber, U., Klatt, D., Papazoglou, S., Zipp, F., Martus, P., Braun, J., Sack, I.: MR-elastography reveals degradation of tissue integrity in multiple sclerosis. Neuroimage **49**(3), 2520–2525 (2010)

[31] Zhang, L.T., Gerstenberger, A., Wang, X., Liu, W.K.: Immersed finite element method. Computer Methods In Applied Mechanics and Engineering **193**(21-22), 2051–2067 (2004)